JOURNAL OF SOLID STATE CHEMISTRY **127,** 267–275 (1996)
ARTICLE NO. 0383

Iron-Promoted Synthesis of Tantalum and Niobium Oxynitrides

Joel D. Houmes and Hans-Conrad zur Loye[1]

Department of Chemistry, Massachusetts Institute of Technology, Cambridge, Massachusetts 02139

Received June 17, 1996; accepted September 18, 1996

$Nb_5N_{6-\delta}O_y$ and $Ta_5N_{6-\delta}O_y$ have been synthesized by reacting iron-containing precursors ($FeMO_4$, FeM_2O_6, Fe_2O_3/M_2O_5, or Fe*M*, *M* − Ta, Nb) with flowing ammonia at 700 and 900°C for the niobium- and tantalum-containing precursors, respectively. It is observed that the oxynitride materials may be synthesized at these temperatures only by using precursors that contain iron. The structures of these materials, which were determined by Rietveld refinement of powder X-ray diffraction data, show marked similarity to the structures of several ternary nitrides synthesized by similar methods. The role of iron in the formation of these materials is discussed. © 1996 Academic Press

INTRODUCTION

The use of oxide precursors has been well documented as an experimentally simple and inexpensive method for the synthesis of a wide variety of nitride and oxynitride products. Of particular note are the recent syntheses of ternary nitrides containing two transition metals starting from the appropriate ternary oxide, demonstrating that complete conversion to a nitride product is possible (1–6). In addition, numerous examples of ammonolysis reactions of ternary oxides, including those containing rare earth elements (7–9) vanadium (10), or alkaline earth elements (11), are known to yield distinct oxynitride products.

Synthesis routes starting from precursors offer several advantages over normal solid state reaction techniques. The reactants in solid state syntheses are usually mixed together manually or mechanically. Consequently, the reaction rate is dependent on (1) the particle size of the reactants, (2) the degree of homogenization achieved on mixing, (3) the intimacy of contact between these grains, and (4) the temperature at which the reaction is carried out (12). On the other hand, precursors can achieve a high degree of homogenization together with intimate contact of the reactants, which result in much higher reaction rates and lower reaction temperatures. In addition, the structure of the precursor may affect product formation (13) and yield phases unattainable by other synthetic routes.

[1] To whom correspondence should be addressed.

In an attempt to synthesize iron tantalum and iron niobium nitride analogues of $FeWN_2$ (1) via ammonolysis of the respective ternary metal oxide precursors, we found that no iron is incorporated in the product. Instead, oxynitride products, $Ta_5N_{6-\delta}O_y$ and $Nb_5N_{6-\delta}O_y$, are formed. We have established that the presence of iron in the precursor is crucial to the formation of these oxynitride phases. In the literature, compounds of the stoichiometry Ta_5N_6 and Nb_5N_6 synthesized by a variety of techniques have been reported. However, oxygen analysis of these compounds was not reported and the complete absence of oxygen from the nitride product is unlikely. The most straightforward method reported for the synthesis of Ta_5N_6 is the ammonolysis of Ta_2O_5 at 975°C (14). However, lower synthesis temperatures lead to a mixed phase product containing Ta_5N_6 and Ta_3N_5. A mixed phase product containing Ta_5N_6 and Ta_3N_5 can also be obtained by decomposing Ta_3N_5 under ammonia at 950°C (14, 15) and the appearance of Ta_5N_6 as an impurity after the decomposition of Ta_3N_5 at higher temperatures has been reported (16). Nitridation of Ta powder at 1200°C under a pressure of 300 bar yields phase-pure Ta_5N_6 (17), while lower pressure nitridation of tantalum metal yields a mixture of phases (18). There have also been several reports of the synthesis of Ta_5N_6 in thin film form through the nitridation of Ta films (19, 20) or by using nitrogen implantation (21); however, all lead to the formation of mixed phase products and in no case do the authors report on the oxygen content of the final products, nor do they provide a structure solution or refinement.

The formation of Nb_5N_6 is much less extensively discussed in the literature. Nb_5N_6 has been reported as a minor product of both the ammonolysis of niobium thin films (22) and as a mixed-phase product in the chemical vapor deposition of films of niobium nitride from $NbCl_5$ in ammonia (23). However, as was the case for tantalum nitride, no oxygen analyses or structure solutions for Nb_5N_6 have been reported. In this paper, we discuss the preparation of $Ta_5N_{6-\delta}O_y$ and $Nb_5N_{6-\delta}O_y$ by the ammonolysis reactions of iron-containing ternary oxide precursors at 900 and 700°C, respectively. These syntheses represent the lowest reported temperatures for the preparation of $Ta_5N_{6-\delta}O_y$

0022-4596/96 $18.00

and $Nb_5N_{6-\delta}O_y$. In addition, the structures of $Ta_5N_{6-\delta}O_y$ and $Nb_5N_{6-\delta}O_y$, as determined by powder X-ray Rietveld refinement, are reported. The apparent catalytic role of iron in effecting nitride formation is also discussed.

EXPERIMENTAL

Synthesis

Precursor preparation. The ternary transition metal oxides used as precursors in this study, $FeNbO_4$, $FeNb_2O_6$, $FeTaO_4$, and $FeTa_2O_6$, were prepared by solid state reaction of the oxides using the method of Koenitzer (24). All starting materials were used as purchased (Fe_2O_3(Cerac, 99.99%), Fe(Aldrich, 99.9%), Ta_2O_5(Johnson–Matthey, 99.9%), Nb_2O_5(Aldrich, 99.9%)). FeMO_4 (M = Ta and Nb) was synthesized by heating an equimolar mixture of Fe_2O_3 and M_2O_5 at 1000°C in air for 48 h. FeM_2O_6 was synthesized by heating a 1 : 1 : 3 molar mixture of Fe_2O_3, Fe, and M_2O_5 in an evacuated quartz tube at 900°C for 48 h. The phase purity of all precursors was confirmed by powder X-ray diffraction.

Ammonolysis reactions. Ammonolysis of $FeNbO_4$, $FeNb_2O_6$, $FeTaO_4$, $FeTa_2O_6$, Nb_2O_5, and Ta_2O_5, as well as of FeTa and FeNb alloys and intimate mixtures of Fe_2O_3/Nb_2O_5 and Fe_2O_3/Ta_2O_5, was carried out in alumina boats which were placed in a quartz flow-through reactor located in a hinged tube furnace. Each sample was heated in flowing ammonia (Airco, Anhydrous 99.99%, 160 cm^3/min, used without further purification) at 5°C/min to 700°C for the niobium-containing precursors and to 900°C for the tantalum-containing precursors. The samples were held at their respective temperatures for ~3.5 days and then rapidly cooled to room temperature by turning off and opening the furnace. Residual iron from the precursor was removed by washing the samples with 5 ml concentrated HCl followed by 5 ml water. Attempts to dissolve the oxynitride products in acids or bases (HCl, HNO_3, aqua regia, H_2SO_4, HF, NaOH) as well as in organic solvents (methanol, ethanol, and acetone) were unsuccessful.

Characterization

Elemental analysis. The nitrogen content of $Ta_5N_{6-\delta}O_y$ and $Nb_5N_{6-\delta}O_y$ was established by C,H,N combustion analysis (Oneida Research Services, Inc.). Metal compositions were determined by Energy Dispersive Spectroscopy (EDS) on a Jeol JSM 6400 scanning electron microscope collected by a Noran Z-max windowless detector with quantification performed using virtual standards on the associated Voyager software. Oxygen content determinations were made by combustion oxygen analysis (Massachusetts Materials Research and Teledyne).

Structural analysis. The polycrystalline samples were structurally characterized using either a Siemens D5000 or a Rigaku RU300 powder X-ray diffractometer operated with Cu$K\alpha$ radiation. Because of the slight air and water sensitivity of $Ta_5N_{6-\delta}O_y$ still containing residual iron, the powdered samples were pressed into the sample holder in an argon-filled glove box and covered with Kaptan film (Du Pont) to limit exposure to air. A powder X-ray diffraction step scan of the iron-containing (unwashed) sample was collected from 14° to 118° 2θ (0.04° 2θ steps) using the Siemens diffractometer. Due to the poor crystallinity of the unwashed $Nb_5N_{6-\delta}O_y$, the powder sample diffracted only marginally better than the Kaptan film used to limit exposure to air. As a result, the background could not be adequately fit using GSAS (25) and further refinement proved futile. Diffraction data for acid-washed samples were collected from 16 to 118° 2θ (0.04 °2θ steps) for $Ta_5N_{6-\delta}O_y$ and from 5 to 140° 2θ (0.04 °2θ steps) for $Nb_5N_{6-\delta}O_y$ using the Rigaku RU300 and Siemens D5000 instruments, respectively. Rietveld refinements of the powder X-ray diffraction data were performed using the General Structure Analysis System (GSAS) refinement package (25). The suggested crystal structure information from the literature was used as a starting model (15).

RESULTS

$Ta_5N_{6-\delta}O_y$ and $Nb_5N_{6-\delta}O_y$ are dark-gray polycrystalline materials. As synthesized from the iron-containing oxide precursors, both samples contained Fe_2N and FeO impurities, which can be removed by washing with concentrated HCl. $Ta_5N_{6-\delta}O_y$ and $Nb_5N_{6-\delta}O_y$ are insoluble in water, polar organic solvents (i.e., methanol, ethanol, and acetone), strong acids, and 6N NaOH. However, exposure to strong acid does result in the incorporation of additional oxygen into the final product. Whether this incorporation takes the form of bulk or of surface oxidation is unclear.

Precursor Experiments

The ammonolysis reactions of the iron-containing ternary oxide precursors lead to the formation of the oxynitrides $Ta_5N_{6-\delta}O_y$ and $Nb_5N_{6-\delta}O_y$ plus the impurities Fe_2N and FeO. None of the iron in the precursor is incorporated into the product, as shown by EDS, which indicates less than 1 atom% iron in the acid-washed samples. Interestingly, the presence of iron in the reaction mixture is essential for the formation of these oxynitride phases. While the iron does not have to be part of the precursor structure, it must be present in the reaction mixture if formation of $Ta_5N_{6-\delta}O_y$ and $Nb_5N_{6-\delta}O_y$ is to be achieved at these temperatures. For example, iron may be added to the reaction mixture by grinding together M_2O_5 (M = Ta or Nb) and Fe_2O_3. In the absence of iron, the formation of other binary nitrides, Ta_3N_5 and Nb_4N_3, is favored.

To test the dependence of the ammonolysis reaction on the starting materials, several different precursor composi-

TABLE 1
Reactions to Investigate the Affect of Iron on Product Formation

Reactants	Ammonolysis conditions	Products
$FeTaO_4$	900°C 4500 min.	$Ta_5N_{5.99}O_{0.01}$ + Fe_2N + FeO
$FeTa_2O_6$	900°C 4500 min.	$Ta_5N_{5.99}O_{0.01}$ + Fe_2N + FeO
$FeTaO_4$	900°C 2186 min.	$Ta_5N_{5.99}O_{0.01}$ + TaON + Fe_2N + FeO
$FeTaO_4$	900°C 900 min.	$Ta_5N_{5.99}O_{0.01}$ + TaON + Fe_2N + FeO
$FeTaO_4$	900°C 5 min.	$FeTa_2O_6$ + Fe_2N
Fe_2O_3 + Ta_2O_5	900°C 4500 min.	$Ta_5N_{5.99}O_{0.01}$ + Fe_2N + FeO
FeTa	900°C 4500 min.	$Ta_5N_{5.99}O_{0.01}$ + Fe_2N + FeO
Ta_2O_5	900°C 4500 min.	Ta_3N_5
Ta_2O_5	900°C 1000 min.	Ta_3N_5
Ta_2O_5	900°C 5 min.	Ta_2O_5 + TaON + Ta_3N_5
$FeNbO_4$	700°C 4500 min.	$Nb_5N_{5.31}O_{0.50}$ + Fe_2N + FeO
$FeNbO_4$	700°C 800 min.	$Nb_5N_{5.31}O_{0.50}$ + $NbN_{0.6}O_{0.3}$ + Fe_2N + FeO
$FeNbO_4$	700°C 5 min.	$FeNb_2O_6$ + $FeNb_{11}O_{29}$ + Fe_2N
$FeNb_2O_6$	700°C 4500 min.	$Nb_5N_{5.31}O_{0.50}$ + Fe_2N + FeO
Fe_2O_3 + Nb_2O_5	700°C 4500 min.	$Nb_5N_{5.31}O_{0.50}$ + Fe_2N + FeO
Nb_2O_5	700°C 4500 min.	$NbN_{0.6}O_{0.2}$ + Nb_4N_3
Nb_2O_5	700°C 1000 min.	$NbN_{0.6}O_{0.3}$
Nb_2O_5	700°C 5 min.	Nb_2O_5 + $NbN_{0.6}O_{0.3}$

tions were prepared and reacted under identical conditions (Table 1). In addition to FeMO_4 (M = Ta, Nb), FeM_2O_6 was prepared, as were mixtures of M_2O_5/FeMO_4 and 1:1 and 1:2 molar mixtures of Fe_2O_3/M_2O_5. In every case, the ammonolysis products were Fe_2N and $M_5N_{6-\delta}O_y$. The ammonolysis of pure Ta_2O_5 or Nb_2O_5, under reaction conditions identical to those used for the iron metallates, yields only Ta_3N_5 and Nb_4N_3/$NbN_{0.6}O_{0.2}$, respectively, as determined by powder X-ray diffraction and visual inspection (Ta_3N_5 is brick red). If Fe_2O_3 is present in the reaction chamber but is separated from M_2O_5 by a small distance, the only observed product is again Ta_3N_5 or Nb_4N_3/$NbN_{0.6}O_{0.2}$, which are the expected products for the ammonolysis of Ta_2O_5 and Nb_2O_5 at these temperatures (22, 26). Since several precursors having varying metal ratios and structures were tried, these factors can be eliminated as causes of the unusual formation of $M_5N_{6-\delta}O_y$ under our reported reaction conditions. One common factor in all the successful reactions was the presence of iron in the reaction mixture.

In order to elucidate the role of iron in influencing the reaction pathway, a series of quenching experiments were carried out (Table 1). From these experiments it is found that the formation of Ta_3N_5 during the ammonolysis of Ta_2O_5 is quite rapid, with detectable product formation after only 5 min at 900°C and going to completion in approximately 12 h (Table 1). When the annomolysis reaction was stopped early, TaON was found to be an intermediate on the reaction pathway. However, it is completely converted to Ta_3N_5 in under 12 h. Early stoppage of the reaction by quenching of the ammonolysis reaction of $FeTaO_4$, on the other hand, results in the formation of $FeTa_2O_6$ and Fe_2N after 5 min at 900°C. After slightly longer reaction times (900 min) TaON, Fe_2N, and $Ta_5N_{6-\delta}O_y$ are formed. Likewise, early stoppage of the ammonolysis reaction of $FeNbO_4$ results in the formation of $FeNb_2O_6$, and Fe_2N (Table 1) after 5 min at 700°C. After slightly longer reaction times (800 min) $NbN_{0.6}O_{0.3}$, Fe_2N, and $Nb_5N_{6-\delta}O_y$ are formed. NbON was not detected in quenching experiments of $FeNbO_4$. However, since TaON demonstrates greater thermal stability and robustness than NbON, the absence of NbON in the quenching is perhaps not surprising. Instead, $NbN_{0.6}O_{0.3}$ is found to be the intermediate. Similarly, when the ammonolysis reaction of Nb_2O_5 is quenched early, the oxynitride $NbN_{0.6}O_{0.3}$ is observed. As the reaction is allowed to proceed further, the oxynitrides are gradually replaced by $M_5N_{6-\delta}O_y$, which suggests that the formation of the binary $M_5N_{6-\delta}$ oxynitrides proceeds via these lower oxynitride intermediates. Since Fe_2N, which is present in the product mixture, decomposes above 300°C and iron oxide reduces to the metal at about 450°C in an ammonia atmosphere, it is reasonable to assume that metallic iron is present under the reaction conditions. Only when the sample is cooled to below 300°C, can Fe_2N begin to form. From these experiments, we hypothesize that the presence of metallic iron in the reaction mixture helps to promote the formation of the $M_5N_{6-\delta}O_y$ phases.

Elemental Analysis of $Ta_5N_{6-\delta}O_y$ and $Nb_5N_{6-\delta}O_y$

$Ta_5N_{6-\delta}O_y$. After the nitride product is washed in concentrated HCl, no iron is detected in the product by EDS.

Nitrogen analysis of the unwashed product mixture yields $N_{Ta} = 8.86$ wt.%, which compares reasonably well with the calculated nitrogen content for Ta_5N_6 (8.50 wt.%). The nitrogen content of the acid-washed product drops significantly ($N_{Ta} - 8.21$ wt.%), presumably due to surface oxidation of the particles or incorporation of oxygen into the oxynitride structure or both as well as the removal of iron nitride from the product mixture. Combustion oxygen analysis of the unwashed product mixtures indicates total oxygen impurities as 0.795 wt.%, whereas a single-phase acid-washed tantantalum oxynitride phase, as expected, contains a larger amount of oxygen ($O_{Ta\text{-washed}} = 2.9$ wt.%). The quantity of FeO and Fe_2N present in the unwashed product mixture was extracted as a weight percentage from a three-phase Rietveld refinement of the powder X-ray diffraction data. Once these values are known, a modified theoretical nitrogen content may be calculated taking into account the amount of nitrogen and oxygen present in Fe_2N and FeO, respectively. The modified nitrogen content (8.86 wt.%) compares very well with the nitrogen content measured by elemental analysis (8.86 wt.%). Given the uncertainty of the phase fraction analysis results using Rietveld refinement, the agreement of the nitrogen analysis with the calculated results is probably not as clear cut as the numbers indicate. However, the exact $Ta_5N_{6-\delta}O_y$ stoichiometry is undoubtedly close to ideal Ta_5N_6 in the unwashed tantalum nitride. With the oxygen and nitrogen that are present as FeO and Fe_2N subtracted, these results yield an overall composition for the unwashed tantalum oxynitride of $Ta_5N_{5.99}O_{0.01}$ (very nearly the idealized composition of Ta_5N_6). After the sample is washed with strong acid, the overall composition becomes $Ta_5N_{4.79}O_{1.81}$.

$Nb_5N_{6-\delta}O_y$. After washing the nitride product in concentrated HCl, no iron is detected in the product by EDS. Nitrogen analysis of the unwashed product mixture ($N_{Nb} - 12.09$ wt.%) is somewhat lower than the calculated values of $N_{Nb} - 13.34$ wt.% for Nb_5N_6. The nitrogen content of the single-phase acid-washed niobium oxynitride drops significantly ($N_{Nb} = 6.4$ wt.%), presumably due to surface oxidation of the particles or incorporation of oxygen into the oxynitride structure or both. Combustion oxygen analysis of the unwashed product mixture indicates a small oxygen impurity (O_{Nb} 2.85 wt.%), while the single-phase acid-washed niobium oxynitride, as expected, contain a larger amount of oxygen (O_{Nb} 6.7 wt.%). Since a Rietveld refinement of the powder X-ray diffraction data for the unwashed sample, was not possible due to sample decomposition, as mentioned earlier, the quantity of FeO and Fe_2N present in the unwashed products was assumed to be identical to that found for $Ta_5N_{6-\delta}O_y$. With the oxygen and nitrogen present as FeO and Fe_2N subtracted, these results yield an estimated overall composition for unwashed niobium oxynitride of $Nb_5N_{5.3}O_{0.5}$. When the samples is washed with strong acid, overall composition becomes $Nb_5N_{2.45}O_{2.25}$.

Structure Refinements

The powder X-ray diffraction patterns of both $Ta_5N_{6-\delta}O_y$ and $Nb_5N_{6-\delta}O_y$ were indexed to a hexagonal

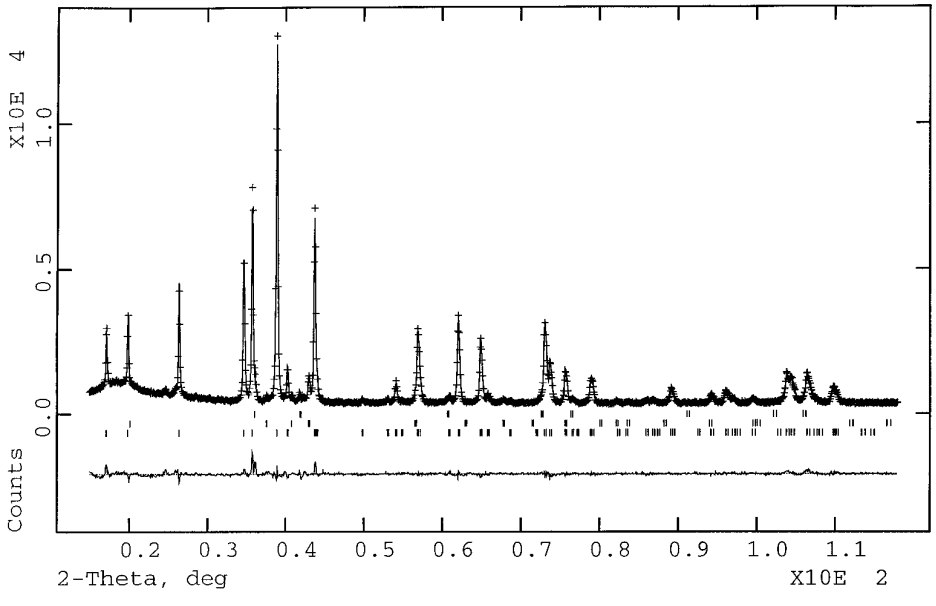

FIG. 1. Observed (dotted) and calculated (solid line) X-ray profile for $Ta_5N_{6-\delta}O_y$. Tick marks below the diffractogram represent allowed Bragg reflections. The difference line, observed minus calculated, is located at the bottom of the figure.

TABLE 2
Rietveld Refinement Data

	Washed $Ta_5N_{6-\delta}O_y$	Unwashed $Ta_5N_{6-\delta}O_y$	Washed $Nb_5N_{6-\delta}O_y$
Powder color	Dark gray	Dark gray	Dark gray
Formula	$Ta_5N_{4.79}O_{1.81}$	$Ta_5N_{5.99}O_{0.01}$	$Nb_5N_{2.45}O_{2.25}$
Formula weight	1000.796	988.805	534.847
Space group	$P6_3/mcm$	$P6_3/mcm$	$P6_3/mcm$
a, Å	5.1803(1)	5.1818(1)	5.2038(3)
c, Å	10.3603(2)	10.3611(3)	10.3714(7)
V, Å	241.077(7)	240.93(1)	243.23(4)
Z	2	2	2
$D_{calc.}$, g/cm^3	13.785	13.629	7.490
2Θ scan range (°)	5–140	15–118	3–118
R_{wp}	6.56%	6.20%	10.84%
R_p	5.03%	4.75%	8.47%
R_{exp}	3.55%	3.82%	4.11%
χ^2	2.910	2.676	7.006

Note. Refinement Rietveld using GSAS with pseudo-Voigt peak shape function.

cell. The structure of $Ta_5N_{6-\delta}O_y$ has been suggested to be in the space group $P6_3/mcm$ and to consist of alternating layers of trigonal prismatically and octahedrally coordinated tantalum atoms with $\frac{1}{3}$ of the octahedral sites vacant (14). More recently, Brokamp and Jacobs (27) have reported a new nitride, $MgTa_2N_3$, which appears to be structurally similar to $Ta_5N_{6-\delta}O_y$ and which is in the space group $P6_3/mcm$ with **a** = 5.205 Å and **c** = 10.425 Å. The reported lattice parameters of $MgTa_2N_3$ and the isostructural $FeTa_2N_3$ (28) and the general shape of the diffraction pattern compare well with those observed for both $Ta_5N_{6-\delta}O_y$ (a = 5.1817(2)Å and c = 10.3610(3)Å) and $Nb_5N_{6-\delta}O_y$ (a = 5.2026(2)Å and c = 10.3667(4)). This model was therefore used as a starting point for structural refinements.

Unwashed $Ta_5N_{6-\delta}O_y$. The powder X-ray diffraction data of $Ta_5N_{6-\delta}O_y$ can be indexed with a hexagonal cell (a = 5.1817(2)Å, c = 10.3610(3)Å).On the basis of systematic absences and the similarity of the data to that exhibited by the compounds listed above, space group $P6_3/mcm$ (No. 193) was chosen. Powder X-ray diffraction patterns calculated for $Ta_5N_{6-\delta}O_y$ in space group $P6_3/mcm$ (using the program DISPOW, part of the NRCVAX crystal structure system(29)) agree well with the observed patterns. The data were refined using the computer program GSAS (25). Structural models for the iron impurity phases (FeO (30) and Fe_2N (31)) were obtained from Structure Reports. The unusual background, due to the presence of the Kaptan film, was described by refining 15 coefficients of a power series. Two parameters were used to refine the unit cell of $Ta_5N_{6-\delta}O_y$ as well as two for Fe_2N and one for FeO. One parameter was included to refine the zero point in 2θ. Three terms were used to refine the phase fractions. A pseudo-Voigt function (32) was used to describe the peak shapes with the following parameters: one Gaussian half-width (W), a Lorentzian half-width, and a Lorentzian strain broadening. The structure refinement of $Ta_5N_{6-\delta}O_y$ included two positional coordinates for the nitrogen atoms as well as one for one of the tantalum atoms, and isotropic thermal displacement factors for each atom. The fractional coordinates and the isotropic thermal parameters for the iron phases were not refined. The refinement converged with R_{wp} = 6.20%, R_p = 4.75%, and χ^2 = 2.676. Figure 1 shows the observed and calculated powder X-ray diffraction patterns along with the residuals for unwashed $Ta_5N_{6-\delta}O_y$ in space group $P6_3/mcm$. The refined lattice parameters and residual values are shown in Table 2; atomic positions and thermal parameters are listed in Table 3a.

Acid-washed $Ta_5N_{6-\delta}O_y$. The powder X-ray diffraction data of acid-washed $Ta_5N_{6-\delta}O_y$ can be indexed with a hexagonal cell (a = 5.1817(2)Å, c = 10.3610(3)Å). On the basis of systematic absences and the similarity of the data to those exhibited by the compounds listed above, space group $P6_3/mcm$ (No. 193) was chosen. Powder X-ray diffraction patterns calculated for $Ta_5N_{6-\delta}O_y$ in space group $P6_3/mcm$ (using the program DISPOW, part of the

TABLE 3a
Atomic Positions of Unwashed $Ta_5N_{6-\delta}O_y$

Metal	Wyckoff	x	y	z	$100*U_{iso}$
Ta(1)	4(d)	1/3	2/3	0	2.36(6)
Ta(2)	6(f)	0.3255(4)	0	1/4	0.67(4)
N	12(k)	0.667(3)	0.667(3)	0.6214(10)	0.7(3)

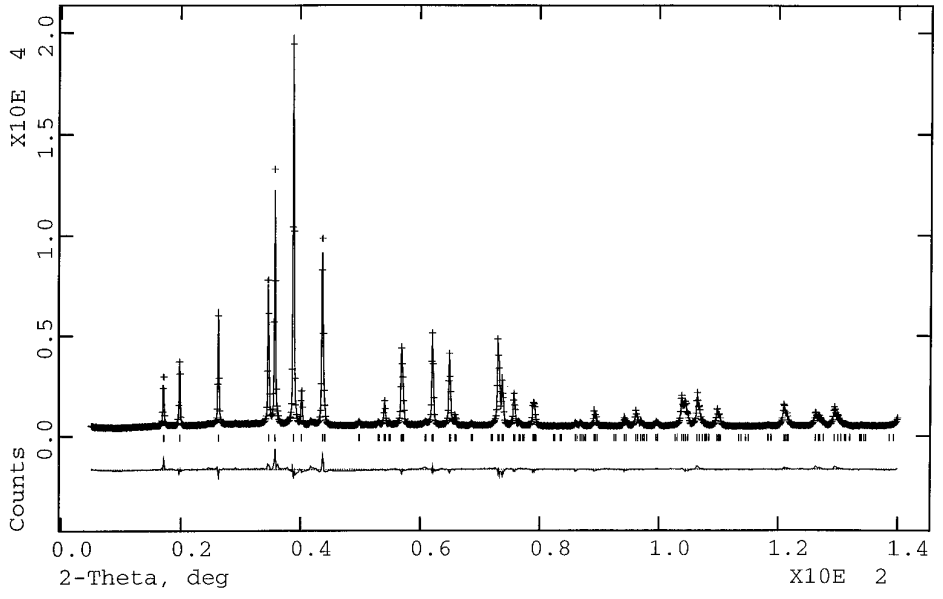

FIG. 2. Observed (dotted) and calculated (solid line) X-ray profile for acid washed $Ta_5N_{6-\delta}O_y$. Tick marks below the diffractogram represent allowed Bragg reflections. The difference line, observed minus calculated, is located at the bottom of the figure.

NRCVAX crystal structure system(29)) agree well with the observed patterns. The data were refined using the computer program GSAS (25). The background was described by refining six coefficients of a power series. Two parameters were used to refine the unit cell. One parameter was included to refine the zero point in 2θ. A pseudo-Voigt function (32) was used to describe the peak shapes with the following parameters: a Lorentzian half-width and strain broadening. The structure refinement of $Ta_5N_{6-\delta}O_y$ included two positional coordinates for the nitrogen atoms as well as one for one of the tantalum atoms, and isotropic thermal displacement factors for each atom. The refinement converged with $R_{wp} = 6.56\%$, $R_p = 5.03\%$, and $\chi^2 = 2.910$. Figure 2 shows the observed and calculated patterns as well as the residuals for acid-washed $Ta_5N_{6-\delta}O_y$ in space group $P6_3/mcm$. Table 3b lists the atomic positions and thermal parameters for $Ta_5N_{6-\delta}O_y$. Little difference is found in the atomic positions between the acid washed and unwashed $Ta_5N_{6-\delta}O_y$.

Acid-washed $Nb_5N_{6-\delta}O_y$. The powder X-ray diffraction data of $Nb_5N_{6-\delta}O_y$ can be indexed with a hexagonal cell ($a = 5.2026(2)$Å, $c = 10.3667(4)$Å). On the basis of systematic absences and the similarity of the data to those exhibited by the compounds listed above, space group $P6_3/mcm$ (No. 193) was chosen. Powder X-ray diffraction patterns calculated for $Nb_5N_{6-\delta}O_y$ in space group $P6_3/mcm$ (using the program DISPOW, part of the NRCVAX crystal structure system (29)) agree well with the observed patterns. The data were refined using the computer program GSAS (25). The background was described by refining six coefficients of a power series. Two parameters were used to refine the unit cell. One parameter was included to refine the zero point in 2θ. A pseudo-Voigt function (32) was used to describe the peak shapes with the following parameters: a Lorentzian half-width and an asymmetric broadening. The structure refinement of $Nb_5N_{6-\delta}O_y$ included two positional coordinates for the nitrogen atoms as well as one for one of the niobium atoms, and isotropic thermal displacement factors for each atom. The refinement converged with $R_{wp} = 10.84\%$, $R_p = 8.47$, and $\chi^2 = 7.006$. It should be noted that several impurity phases are present in the powder X-ray diffraction pattern of $Nb_5N_{6-\delta}O_y$. The small peak at 42° arises from the presence of $NbN_{0.6}O_{0.3}$, apparently an intermediate on the reaction pathway. This phase can be eliminated through longer reaction times. However, longer reaction times lead to the formation of hexagonal δ-NbN and ε-NbN, which result from a collapse of the $Nb_5N_{6-\delta}O_y$ structure and occupancy of all the metal sites. All of these impurity phases have diffraction peaks which overlap with those from $Nb_5N_{6-\delta}O_y$. Because of the structural similarity to the product and the very small amount of the impurities, multiple phase refinement to include the presence of the impu-

TABLE 3b
Atomic Positions of Acid Washed $Ta_5N_{6-\delta}O_y$

Metal	Wyckoff	x	y	z	$100*U_{iso}$
Ta(1)	4(d)	1/3	2/3	0	2.33(4)
Ta(2)	6(f)	0.3236(2)	0	1/4	0.53(2)
N	12(k)	0.667(2)	0.667(2)	0.6230(5)	1.3(2)

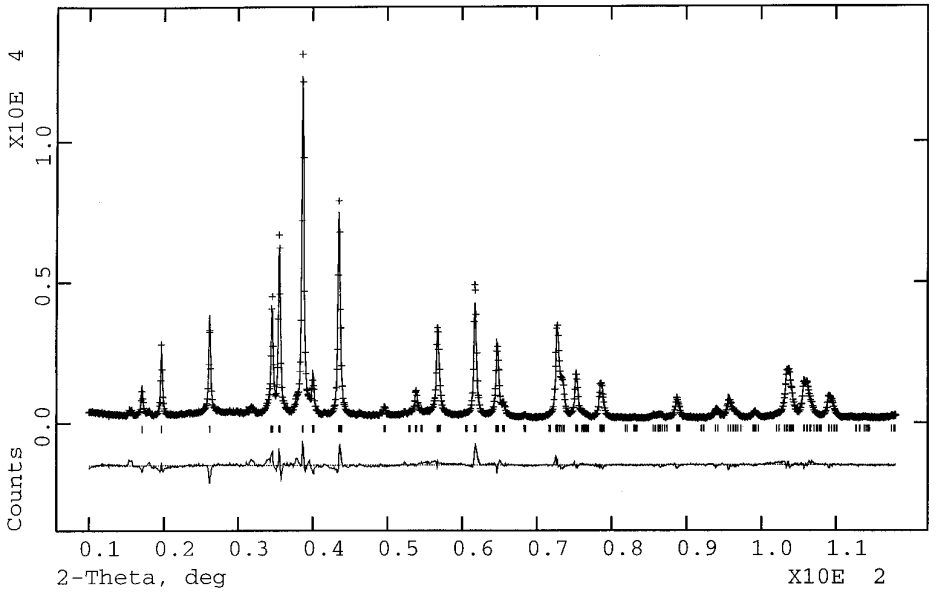

FIG. 3. Observed (dotted) and calculated (solid line) X-ray profile for acid washed $Nb_5N_{6-\delta}O_y$. Tick marks below the diffractogram represent allowed Bragg reflections. The difference line, observed minus calculated, is located at the bottom of the figure.

rity phases failed. The presence of the impurity phases in the Rietveld refinement presented undoubtedly lead to inflated values of R_{wp}, R_p, and χ^2. Figure 3 shows the observed and calculated diffraction patterns along with the residuals for acid-washed $Nb_5N_{6-\delta}O_y$ in space group $P6_3/mcm$. Table 3c lists the atomic positions and thermal parameters for $Nb_5N_{6-\delta}O_y$.

DISCUSSION

The structure of $M_5N_{6-\delta}O_y$ (M = Ta and Nb) is quite similar to structures exhibited by many ternary molybdenum and tungsten nitride materials (1–6) as well as by some intercalated dichalcogenide materials (33–35) and the recently reported carbide $ScCrC_2$ (36). It consists of close-packed nitrogen/oxygen layers with the metal in alternating layers of octahedral and trigonal prismatic coordination as shown in Fig. 4. Tantalum occupies all of the trigonal primatic sites and 2/3 of the octahedral sites, with the remaining octahedral sites vacant. The atom stacking can be denoted **AbAcBaBcA** (capital letters denote anion stacking, lower case letters denote metal stacking). Interatomic distances are reported in Table 4. The metal–nitrogen distances found in both $Ta_5N_{6-\delta}O_y$ and $Nb_5N_{6-\delta}O_y$ (unwashed Ta–N: 2.162(8), 2.140(8), 2.224(12)Å; Nb–N: 2.170(6), 2.276(9), 2.148(6)Å) are comparable to the metal–nitrogen distances found in binary nitrides and in other oxynitrides of tantalum and niobium (e.g., β-Ta_2N, 2.08Å (37); Ta_3N_5, 2.09Å (37); TaON, 2.09Å (37); β-Nb_2N, 2.15Å (37); γ-Nb_4N_3, 2.19Å (37); NbON, 2.09Å (37)). The M–N distance comparisons are more reliable in the case of $Ta_5N_{6-\delta}O_y$ because the Nb–N (and Ta–N distances for the acid washed $Ta_5N_{6-\delta}O_y$) are presumably affected by oxygen introduced in the acid-washing step.

TABLE 3c
Atomic Positions of $Nb_5N_{6-\delta}O_y$

Metal	Wyckoff	x	y	z	$100*U_{iso}$
Nb(1)	4(d)	1/3	2/3	0	0.48(6)
Nb(2)	6(f)	0.3254(4)	0	1/4	0.11(4)
N	12(k)	0.676(2)	0.676(2)	0.6189(7)	1.3(3)

It is particularly interesting to note the structural relationships between these oxynitrides and several ternary nitrides which have recently been synthesized, $FeWN_2$, α, β-$MnWN_2$, $(Fe_{0.8}Mo_{0.2})MoN_2$, and $LiMoN_2$. The similarity between the ternary transition metal nitride and the oxynitride compounds can be emphasized by utilizing the notation $(M_{0.67}\square_{0.33})MN_{2-\delta}O_y$ (M = Ta or Nb; $\square$ = vacancy), a similarity which is particularly striking for the unwashed tantalum oxynitride, which, if the small degree (<0.01 equivalents) of oxygen ''contamination'' is ignored, may be written as $(Ta_{0.67}\square_{0.33})TaN_{2-\delta}$. The presence of this vacancy in the octahedral layer can be understood by examining some ternary transition metal nitrides which have similar structures. Mössbauer spectroscopy measurements performed on $FeWN_2$ indicate that the iron in the octahedral site has a valence of +2 (38). Thus, formally, $FeWN_2$ has WN_2^{-2} trigonal prismatic layers which are isoelectronic with the WS_2 layers present in tungsten disulfide. If similar TaN_2^{-2} layers in $(Ta_{0.67}\square_{0.33})TaN_{2-\delta}$ are assumed to be iso-

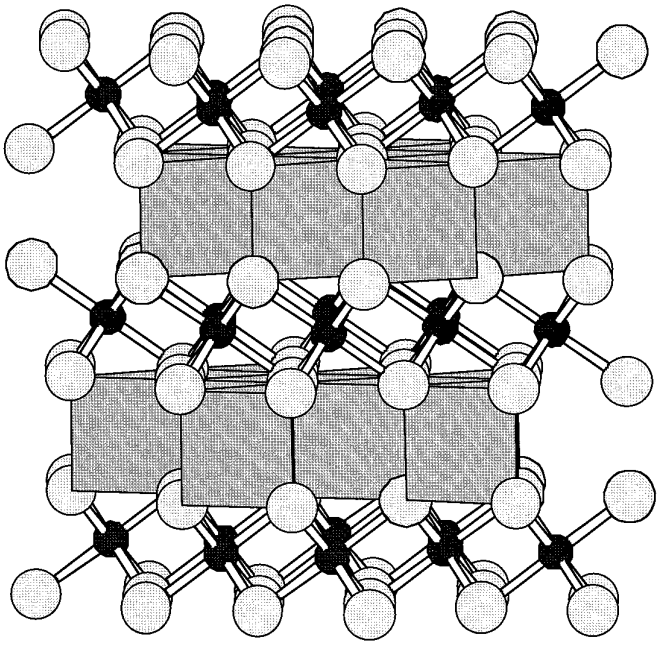

FIG. 4. Proposed structure for $Ta_5N_{6-\delta}O_y$ and $Nb_5N_{6-\delta}O_y$. Trigonal prismatic tantalum/niobium is shown as filled polyhedra. The octahedral tantalum/niobium and all the nitrogen/oxygen positions are indicated by a ball and stick representation. The small dark gray spheres represent tantalum/niobium atoms and the large light gray spheres represent nitrogen/oxygen atoms.

electronic with TaS_2, one +2 cation must be incorporated for every trigonal prismatic tantalum to maintain charge balance. In $(Ta_{0.67}\square_{0.33})TaN_{2-\delta}$, the unit cell has three octahedral sites and 3 trigonal prismatic tantalum sites per layer. Given the preference for Ta(III) over Ta(II), one third of the octahedral sites in this structure must remain vacant in order to maintain charge balance with Ta(III).

Additional structural similarities between these oxynitride compounds and the transition metal dichalcogenides and the ternary transition metal nitrides are present. Contractions of the **c**-axis in the MS_6 trigonal prisms are observed in the structures of the transition metal dichalcogenides and result in increased metal–chalcogenide bond covalency and chalcogenide–chalcogenide interactions (39, 40). Similarly, the trigonal prismatic MN_6 units in some ternary transition metal nitrides are contracted along the **c** axis as a result of increased metal–nitrogen bond covalency as indicated by band structure calculations performed on $LiMoN_2$ (41). Contractions of the trigonal prismatic unit in $Ta_5N_{6-\delta}O_y$ and $Nb_5N_{6-\delta}O_y$ are observed, presumably again due to increased covalency in the metal–heteroatom bond. The nitrogen–nitrogen distance along the **c** axis of the trigonal prism (2.67 Å for the unwashed tantalum compound, 2.75 Å for the washed niobium compound) is among the shortest nitrogen–nitrogen distances reported for nitride compounds, although the N–N distance in the niobium oxynitride is undoubtedly affected by the presence of oxygen. In any case, these distances are significantly shorter than the nitrogen–nitrogen distances within the **ab** plane (2.974 Å for the unwashed tantalum compounds, 2.987 Å for the washed niobium compound).

Nitrogen analysis, oxygen analysis, and Rietveld refinement indicated that a phase of composition nearly Ta_5N_6 is present before the tantalum oxide ammonolysis product is washed with HCl. However, the analogous Nb_5N_6 apparently does not form. Instead, a structurally similar oxynitride forms, presumably due to the lower reaction temperature used in the ammonolysis of the niobium precursor. Attempts to run the ammonolysis of the niobium precursors at temperatures above 700°C result in the formation of lower binary nitrides (NbN and Nb_4M_3).

Role of Iron in Product Formation

Table 1 lists a series of reactions used to elucidate the role of iron in product formation. In the absence of iron, the oxynitride intermediates are observed only fleetingly, suggesting that the role of the iron is to stabilize these species. In fact, the apparent necessity of the presence of iron in the formation of $Ta_5N_{6-\delta}O_y$ and $Nb_5N_{6-\delta}O_y$ suggests a possible catalytic role for iron. In the quenching experiments of the iron containing precursors, iron nitride (Fe_2N) is found in the product after only 5 min at the reaction temperature (Table 1), indicating a loss of iron/iron oxide

TABLE 4
Interatomic Distances

	Unwashed $Ta_5N_{6-\delta}O_y$ *P*6$_3$/*mcm*	Washed $Ta_5N_{6-\delta}O_y$ *P*6$_3$/*mcm*	$Nb_5N_{6-\delta}O_y$ *P*6$_3$/*mcm*
M(1)–*M*(1)	2.99172(7) Å	2.99081(2) Å	3.0044(2) Å
M(1)–*M*(2)	3.1249(5) Å	3.1274(3) Å	3.1333(7) Å
M(2)–*M*(2)	3.028(2), 2.921(3) Å	3.036(1), 2.903(2) Å	3.047(2), 2.921(4) Å
M(1)–N	2.141(8) Å	2.145(5) Å	2.141(7) Å
M(2)–N	2.161(8), 2.225(12) Å	2.152(5), 2.232(8) Å	2.174(7), 2.290(10) Å
N–N	3.00(1), 2.97(2), 2.67(2) Å	3.004(7), 2.96(1), 2.66(1) Å	3.05(1), 2.92(2), 2.75(2) Å

from the precursor. Since both Fe_2N and Fe_2O_3 are unstable above ~450°C, the reduction of iron in the precursor to iron metal at the reaction dwelling temperature is suggested. The iron can agglomerate in the reaction mixture to form finely divided particles, whose presence is demonstrated by the strongly exothermic reaction which results if the sample is exposed to air without sufficient equilibriation time under 300°C to allow the formation of a protective Fe_2N coating. Iron has been reported to affect the ammonolysis of other materials. For example, Glasson reports that iron impurities appear to accelerate the nitridation of Si, W, Mo, and other elements (42). In the experiments reported in this paper, it appears to slow the formation of the oxynitride intermediate and affect the formation of $M_5N_{6-\delta}O_y$ from the oxynitride intermediate.

The role of intermediate oxynitrides in affecting the formation of specific products has been observed in other instances. Jaggers *et al.* studied the ammonolysis reaction of ammonium molybdates and found that the reaction product, MoN or Mo_2N, was dependent on the type of molybdate precursor employed and on the temperature at which the oxynitride intermediate was formed (13). In this study, not only is the formation of TaON much slower than in the ammonolysis of Ta_2O_5, but the conversion of the TaON intermediate to the nitride product takes much longer, with complete conversion taking ~3.5 days (Table 1). Likewise, in the ammonolysis of iron-containing precursors to form $Nb_5N_{6-\delta}O_y$, the formation of the oxynitride intermediate is also slower than in the ammonolysis of Nb_2O_5. However, some oxynitride remains in the product mixture even after 4500 min at 700°C. The persistance of a lower niobium oxynitride in the ammonolysis of niobium oxide could be explained by the lower reaction temperature relative to the ammonolysis of tantalum oxide, which could slow the exchange of nitrogen into the material. Also, very few binary nitride or oxynitride materials are known which contain niobium with a formal oxidation state of greater than 3, which could also explain the persistance of the lower oxynitride in the ammonolysis of Nb_2O_5. Regardless, the presence of iron in the reaction mixture dramatically effects the synthetic pathway in these ammonolysis reactions, a fact which warrants further investigation in the future.

ACKNOWLEDGMENTS

Acknowledgment is made to the Donors of the Petroleum Research Fund and the National Science Foundation through Grant DMR: 9419603. JDH thanks 3M for financial support.

REFERENCES

1. D. S. Bem, C. M. Lampe-Önnerud, H. P. Olsen, and H.-C. zur Loye, *Inorg. Chem.* **35,** 581 (1996).
2. D. S. Bem, H. P. Olsen, and H.-C. zur Loye, *Chem. Mater.* **7,** 1824 (1995).
3. D. S. Bem and H.-C. zur Loye, *J. Solid State Chem.* **104,** 467 (1993).
4. J. Houmes, D. Bem, and H.-C. zur Loye, *in* "Materials Research Society Symposium Proceedings," Vol. 327, p. 153, 1994.
5. S. H. Elder, F. J. DiSalvo, and L. H. Doerrer, *Chem. Mater.* **4,** 928 (1992).
6. P. Subramanya Herle, M. S. Hegde, N. Y. Vasanthacharya, J. Gopalakrishnan, and G. N. Subbanna *J. Solid State Chem.* **112,** 208 (1994).
7. R. Marchand, P. Antoine, and Y. Laurent *J. Solid State Chem.* **107,** 34 (1993).
8. F. Pors, R. Marchand, and Y. Laurent, *J. Solid State Chem.* **107,** 39 (1993).
9. P. Bacher, P. Antoine, R. Marchand, P. L'Haridon, Y. Laurent, and G. Roult, *J. Solid State Chem.* **77,** 67 (1988).
10. C. C. Yu and S. T. Oyama, *J. Solid State Chem.* **116,** 205 (1995).
11. J. Grins and G. Svensson, *Mater. Res. Bull.* **29,** 801 (1994).
12. A. R. West, "Solid State Chemistry and Its Applications," p. 734. Wiley, NewYork, 1984.
13. C. H. Jaggers, N.M. James, and A. M. Stacy, *Chem. Mater.* **2,** 150 (1990).
14. A. Fontbonne and J.-C. Gilles, *Rev. Int. Hautes Temp. Refract.* **6,** 181, 1969.
15. J.-C. Gilles *C.R. Acad. Sci. Paris Ser. C.* **266,** 546 (1968).
16. A. Yajima, R. Matsuzaki, and Y. Saeki, *Denki Kagaku Oyobi Kogyo Botsuri Kagaku* **51,** 676 (1983).
17. A. Vendl, *Monatsh. Chem.* **109,** 1009 (1978).
18. G. Brauer and E. Mohr-Rosenbaum, *Monatsh. Chem.* **102,** 1311 (1971).
19. N. Terao, *Jpn. J. Appl. Phys.* **10,** 248 (1971).
20. P. T. Dawson and S. A. J. Stazyk, *J. Vac. Sci. Technol.* **20,** 966 (1992).
21. P. M. Raole, A.M. Narsale, D. C. Kothari, W. V. Gogawale, L. Guzman, and M. Dapor, *Mater. Sci. Eng. A* **115,** 73 (1989).
22. N. Terao, *J. Less-Common Met.* **23,** 159 (1971).
23. G. Oya and Y. Onodera, *J. Appl. Phys.* **45,** 1389 (1974).
24. J. Koenitzer, B. Khazai, J. Hormadaly, R. Kershaw, K. Dwight, and A. Wold, *J. Solid Chem.* **35,** 128 (1980).
25. A. C. Larson and R. B. von Dreele, *in* "GSAS, Los Alamos National Laboratory, Los Alamos, 1990."
26. V. G. Brauer, J. Weidlein, and J. Strahle, *Z. Anorg. Allg. Chem.* **348,** 298 (1966).
27. T. Brokamp and H. Jacobs, *J. Alloys Compounds* **183,** 325 (1992).
28. N. Schonberg, *Acta Chem. Scand.* **8,** 213 (1954).
29. A. C. Larson, F. L. Lee, Y. Le Page, M. Webster, J. P. Charland, and E. J. Gabe, *in* "Chemistry Division, NRC, Ottawa, Canada, K1A 0R6."
30. *Struct. Rep.* **24,** 315.
31. *Struct. Rep.* **18,** 166.
32. P. Thompson, D. E. Cox, and J. B. Hastings, *J. Appl. Crystallogr.* **20,** 79 (1987).
33. F. J. Di Salvo, B. G. Bagley, J. M. Voorhoeve, and J. V. Waszczak, *Phys. Chem. Solids* **34,** 1357 (1973).
34. M. S. Whittingham, *Prog. Solid State Chem.* **12,** 41 (1978).
35. J. Rouxel, *in* "Intercalated Layered Materials" (F. Levy, Ed.), 1st ed.; Vol. 6, p. 201. Reidel, Hingham, MA, 1979.
36. R. Pöttgen, A. M. Witte, W. Jeitschko, and T. Ebel, *J. Solid State Chem.* **119,** 324 (1995).
37. N. E. Brese and M. O'Keefe, *Struct. Bonding* **79,** 307 (1992).
38. D. S. Bem, J. D. Houmes, and H.-C. zur Loye, *in* "MRS Covalent Ceramics II: Non Oxides; Boston, 1993," Vol. 327, p. 165.
39. H. W. Myron, *Physica B* **105,** 120 (1981).
40. R. H. Friend and A. D. Yoffe, *Adv. Phys.* **36,** 1 (1987).
41. D. J. Singh, *Phys. Rev. B.* **46,** 9332 (1992).
42. D. R. Glasson and S. A. A. Jayaweera, *J. Appl. Chem.* **18,** 65 (1968).